9488 *Biochemistry* **2010,** *49,* 9488–9497
DOI: 10.1021/bi1013134

BIOCHEMISTRY
including biophysical chemistry & molecular biology
Article

The α-Helical C-Terminal Domain of Full-Length Recombinant PrP Converts to an In-Register Parallel β-Sheet Structure in PrP Fibrils: Evidence from Solid State Nuclear Magnetic Resonance[†]

Robert Tycko,*[,‡] Regina Savtchenko,[§] Valeriy G. Ostapchenko,[§] Natallia Makarava,[§] and Ilia V. Baskakov[§]

[‡]*Laboratory of Chemical Physics, National Institute of Diabetes and Digestive and Kidney Diseases, National Institutes of Health, Bethesda, Maryland 20892-0520, United States, and* [§]*Center for Biomedical Engineering and Technology, Department of Anatomy and Neurobiology, University of Maryland, Baltimore, Maryland 21201, United States*

Received August 16, 2010; Revised Manuscript Received October 5, 2010

ABSTRACT: We report the results of solid state nuclear magnetic resonance (NMR) measurements on amyloid fibrils formed by the full-length prion protein PrP (residues 23−231, Syrian hamster sequence). Measurements of intermolecular $^{13}C-^{13}C$ dipole−dipole couplings in selectively carbonyl-labeled samples indicate that β-sheets in these fibrils have an in-register parallel structure, as previously observed in amyloid fibrils associated with Alzheimer's disease and type 2 diabetes and in yeast prion fibrils. Two-dimensional $^{13}C-^{13}C$ and $^{15}N-^{13}C$ solid state NMR spectra of a uniformly ^{15}N- and ^{13}C-labeled sample indicate that a relatively small fraction of the full sequence, localized to the C-terminal end, forms the structurally ordered, immobilized core. Although unique site-specific assignments of the solid state NMR signals cannot be obtained from these spectra, analysis with a Monte Carlo/simulated annealing algorithm suggests that the core is comprised primarily of residues in the 173−224 range. These results are consistent with earlier electron paramagnetic resonance studies of fibrils formed by residues 90−231 of the human PrP sequence, formed under somewhat different conditions [Cobb, N. J., Sonnichsen, F. D., McHaourab, H., and Surewicz, W. K. (2007) *Proc. Natl. Acad. Sci. U.S.A. 104*, 18946−18951], suggesting that an in-register parallel β-sheet structure formed by the C-terminal end may be a general feature of PrP fibrils prepared in vitro.

PrP is a 210-residue prion protein whose aberrant aggregation leads to infections neurodegenerative diseases in higher animals (*1*). Although it has not been definitively established that the infectious or neurotoxic form of PrP is an amyloid fibril (*2*), the self-propagating nature of the infectious form (commonly called PrP^{Sc}, with Sc representing scrapie) can be readily understood if PrP^{Sc} has a molecular structure that at least resembles structures of amyloid fibrils (*3*). In particular, the existence of multiple, distinct, self-propagating strains or variants of PrP^{Sc} (*4*, *5*) is consistent with the observation of self-propagating polymorphs of amyloid fibrils, such as the β-amyloid fibrils associated with Alzheimer's disease (*6*, *7*). Distinct strains of yeast prions have also been attributed to self-propagating amyloid polymorphism (*8*−*11*).

Amyloid fibrils are filamentous peptide or protein aggregates containing cross-β structures, i.e., ribbonlike β-sheets in which the β-strands run approximately perpendicular to the long axis and interstrand hydrogen bonds run approximately parallel to the long axis. Full-length recombinant PrP and various PrP fragments are capable of forming amyloid fibrils in vitro (*12*−*20*), and recombinant PrP fibrils are cytotoxic (*21*). Fibrils formed by $PrP_{127-147}$ and $PrP_{106-126}$ have been shown by solid state NMR[1] to contain in-register parallel β-sheets (*18*, *20*), while evidence of antiparallel β-sheets in $PrP_{109-122}$ fibrils (*16*) and against in-register parallel β-sheets in PrP_{89-143} fibrils (*14*) has also been reported (with PrP_{n-m} representing residues $n-m$ of full-length PrP). Solid state NMR measurements on PrP_{23-144} fibrils indicate that the structured core involves only a relatively short segment, namely, residues 112−141 (*15*, *19*), although the type of β-sheets within these fibrils has not yet been reported. Molecular structural studies of amyloid fibrils formed by PrP_{90-231} or PrP_{23-231} (the full-length protein after cleavage of an N-terminal signal peptide) have been limited to lower-resolution techniques, including atomic force microscopy (AFM) and electron microscopy (EM) (*12*, *13*, *22*, *23*), hydrogen−deuterium (H−D) exchange (*24*), proteolysis (*13*), electron paramagnetic resonance (EPR) (*25*), and Fourier transform infrared spectroscopy (FTIR) (*13*, *26*). Recombinant full-length PrP fibrils are also polymorphic, with the predominant fibril morphology being dependent on growth conditions such as the intensity of agitation during incubation. Baskakov and co-workers have described two morphologies of fibrils formed by residues PrP_{23-231}, called R and S fibrils, which differ in their appearance in AFM and EM images (*17*) as well as in the conformational properties probed by FTIR, H−D exchange, proteolysis patterns, X-ray

[†]This work was supported by the Intramural Research Program of the National Institute of Diabetes and Digestive and Kidney Diseases of the National Institutes of Health (NIH) and by NIH Grant NS045585 to I. V.B.

*To whom correspondence should be addressed. Phone: (301) 402-8272. Fax: (301) 496-0825. E-mail: robertty@mail.nih.gov.

[1]Abbreviations: NMR, nuclear magnetic resonance; EM, electron microscopy; FTIR, Fourier transform infrared; H−D, hydrogen−deuterium; EPR, electron paramagnetic resonance; MES, 2-(*N*-morpholino)ethanesulfonic acid; MAS, magic-angle spinning; 2D, two-dimensional; rf, radiofrequency; PITHIRDS-CT, constant-time π pulse recoupling; fpRFDR, finite-pulse radiofrequency-driven recoupling; TPPM, two-pulse phase-modulated; NCACX, 2D $^{15}N-^{13}C_\alpha/^{13}C_X$ spectrum; NCOCX, 2D $^{15}N-^{13}CO/^{13}C_X$ spectrum; INEPT, insensitive nuclei enhanced by polarization transfer; MCA/SA, Monte Carlo/simulated annealing; PK, proteinase K; TMS, tetramethylsilane.

 Published on Web 10/06/2010

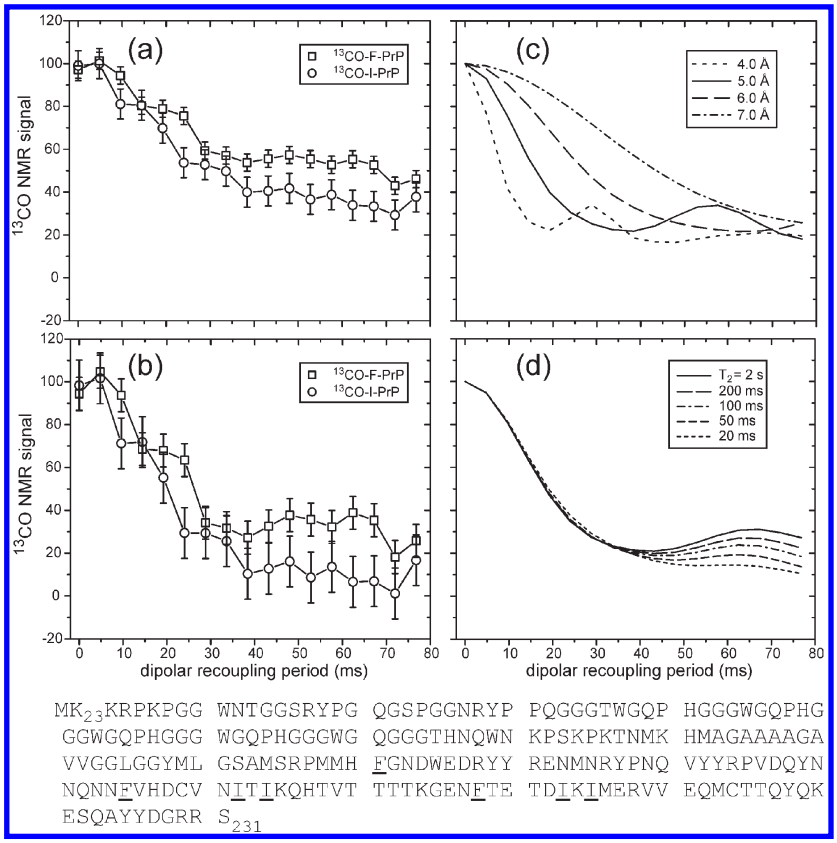

FIGURE 1: (a) Experimental measurement of intermolecular $^{13}C-^{13}C$ dipole−dipole couplings using the PITHIRDS-CT solid state NMR technique, for ^{13}CO-F-PrP and ^{13}CO-I-PrP fibrils (□ and ○, respectively). Positions of labeled Phe and Ile residues are underlined in the PrP$_{23-231}$ sequence at the bottom of the figure. Error bars represent the root-mean-squared noise in the NMR signals. Lines are guides to the eye. (b) Experimental PITHIRDS-CT data after correction for natural-abundance ^{13}C signal contributions as explained in the text. (c) Simulated PITHIRDS-CT curves for linear chains of dipole-coupled ^{13}C nuclei with the indicated spacings. T_2 relaxation is not included. (d) Simulated PITHIRDS-CT curves for dipole-coupled ^{13}C nuclei with a 4.8 Å spacing and with indicated values of the transverse relaxation time T_2.

fiber diffraction, and dye binding (*27*). In the PrP$_{90-231}$ fibrils prepared by Surewicz and co-workers, the fibril core is comprised approximately of residues 160−220, which form in-register parallel β-sheets according to EPR measurements of spin-labeled samples (*25*).

In this paper, we report the results of solid state NMR measurements on recombinant PrP$_{23-231}$ amyloid fibrils, specifically the R morphology of these fibrils (*17*, *27*). The principal conclusions are that these fibrils contain in-register parallel β-sheets and that the structurally ordered fibril core includes the C-terminal segment, approximately residues 175−225, which includes the second and third α-helices of monomeric PrP (*28*, *29*). Only a subset of residues within this segment contribute to solid state NMR signals, however, suggesting that structurally ordered subsegments (presumably β-strands) coexist with disordered and dynamic subsegments (presumably loops). The Discussion addresses how these results relate to previous studies of PrP fibrils and PrP^{Sc}.

MATERIALS AND METHODS

Expression of Uniformly and Selectively Labeled PrP$_{23-231}$ and Fibril Formation. Uniformly ^{15}N- and ^{13}C-labeled recombinant Syrian hamster PrP$_{23-231}$ [U-^{15}N,^{13}C-PrP (sequence in Figure 1)] was expressed as described previously (*30*), with the modification that, after transformation, cells were grown on ^{15}N- and ^{13}C-enriched (98% enrichment) Spectra-9 bacterial growth medium. PrP$_{23-231}$ samples labeled selectively with [1-^{13}C]isoleucine (^{13}CO-I-PrP) and with [1-^{13}C]phenylalanine (^{13}CO-F-PrP) were expressed in BL21 Star *Escherichia coli* as described by Baxa et al. (*31*) in synthetic medium with the composition described by Cai et al. (*32*) with a minor modification (10 mM $MgSO_4$ instead of K_2SO_4). Spectra-9 medium, [1-^{13}C]isoleucine, and [1-^{13}C]phenylalanine were purchased from Cambridge Isotope Laboratories.

Lyophilized labeled protein was dissolved in 50 mM 2-(*N*-morpholino)ethanesulfonic acid (MES) buffer (pH 6.0) immediately before use. The protein concentration was determined by measuring the absorbance at 280 nm. Fibrils were formed at 37 °C in the reaction mixture of 0.5 mg/mL labeled PrP$_{23-231}$, 50 mM MES (pH 6.0), and 2 M guanidinium chloride, in a 15 or 50 mL centrifuge tube with a conical bottom (Sarstedt), under continuous 24 rpm rotation using a Clay Adams Nutator (model 1105) for several days. Formation of fibrils was monitored by a thioflavin T binding assay and confirmed by EM as previously described (*33*). The fibrils were dialyzed overnight into 10 mM Tris (pH 7.5) and centrifuged for 2 h at 10000*g* to obtain a slurry of concentrated fibrils.

EM and AFM images of isotopically labeled PrP$_{23-231}$ fibrils are shown in Figure S1 of the Supporting Information. The morphologies of these fibrils match those of the R fibrils described previously (*17*).

Atomic Force Microscopy of PrP Fibrils. Amyloid fibrils produced from uniformly or selectively labeled PrP$_{23-231}$ were dialyzed for 4 h against 10 mM sodium acetate buffer (pH 5.0) with one buffer change after 2 h. Ten microliters of each sample (PrP$_{23-231}$ concentration of ~10 μg/mL) was applied on freshly

cleaved mica, incubated for 5 min at room temperature for fibril adsorption, gently washed with ultrapure water, and left to dry on the bench. AFM imaging was performed using a Pico LE system (Agilent Technologies). The AFM scanner was equipped with a PPP-NCH silicon cantilever (Nanosensors) and operated in tapping mode at the resonant frequency of approximately 300 kHz. The images (512 pixels × 512 pixels) were collected at a scan rate of one line per second.

Solid State NMR Measurements. All NMR measurements were performed at room temperature. Measurements of intermolecular $^{13}C-^{13}C$ dipole−dipole couplings in Figure 1 were performed on the ^{13}CO-F-PrP and ^{13}CO-I-PrP fibril samples with the PITHIRDS-CT technique (*34*) at a 399.2 MHz ^{1}H NMR frequency (100.4 MHz ^{13}C NMR frequency) with magic-angle spinning (MAS) at 20.00 kHz, using a Varian InfinityPlus spectrometer and a Varian 3.2 mm MAS probe. Radiofrequency (rf) pulse sequence conditions were as previously described (*6*, *34*−*36*), with pulsed spin-locking to enhance the signal-to-noise ratio (*37*) and active MAS synchronization with tachometer filtering to permit a 76.8 ms $^{13}C-^{13}C$ recoupling period. Samples were lyophilized for these measurements and amounted to approximately 2.0 mg for ^{13}CO-F-PrP and 0.7 mg for ^{13}CO-I-PrP, packed in thick-wall 3.2 mm MAS rotors with additional Teflon spacers to contain the samples in the center of the probe's rf coil. A total of 800 scans was acquired for each PITHIRDS-CT data point, with a 4.0 s recycle delay. Test measurements on U-^{15}N,^{13}C-PrP fibrils confirmed that lyophilization did not disrupt the PrP fibril structure (i.e., did not alter the ^{13}C MAS NMR spectrum), consistent with previous observations for various other amyloid fibrils (*38*−*40*). PITHIRDS-CT data for ^{13}CO-F-PrP and ^{13}CO-I-PrP fibrils after rehydration by addition of 3 μL of H_2O to the MAS rotors are shown in Figure S2 of the Supporting Information.

Two-dimensional (2D) NMR spectra of U-^{15}N,^{13}C-PrP fibrils were obtained at a 747.6 MHz ^{1}H NMR frequency (188.0 MHz ^{13}C and 75.8 MHz ^{15}N NMR frequencies) and a 17.00 kHz MAS frequency, using a Varian Infinity spectrometer and a 1.8 mm MAS probe constructed in the group of A. Samoson (National Institute of Chemical Physics and Biophysics, Tallinn, Estonia). The U-^{15}N,^{13}C-PrP fibril sample (approximately 5 mg of protein) was pelleted directly into the MAS rotor without lyophilization.

The 2D $^{13}C-^{13}C$ NMR spectrum in Figure 3 was acquired with a 2.82 ms mixing period, using finite-pulse radiofrequency-driven recoupling (fpRFDR) (*41*, *42*). ^{13}C π pulses in the fpRFDR period were 18.00 μs at a carrier frequency of 69 ppm. Two-pulse phase-modulated (TPPM) decoupling (*43*) was applied in the t_1 and t_2 periods, with a 100 kHz ^{1}H rf field, a 20.0 μs t_1 increment, and 200 t_1 points. A total of 2496 scans was acquired for each complex t_1 point, with a 1.0 s recycle delay. 2D $^{15}N-^{13}C$ NMR spectra (NCACX and NCOCX) shown in Figure 4 were acquired with mixing periods consisting of a 4.0 ms frequency-selective $^{15}N-^{13}C$ cross-polarization period (*44*) followed by a 2.82 ms fpRFDR period and with 45.5 μs t_1 increments and 150 t_1 points. For the NCACX spectrum, the ^{13}C carrier frequency was 44 ppm and ^{13}C π pulses were 20.0 μs in duration in the fpRFDR period. For the NCOCX spectrum, the ^{13}C carrier frequency was 105 ppm and ^{13}C π pulses were 10.0 μs in duration in the fpRFDR period. A total of 3584 and 5120 scans was acquired for each complex t_1 point in NCACX and NCOCX measurements, respectively, with a 1.0 s recycle delay.

The ^{13}C-detected 2D $^{1}H-^{13}C$ NMR spectrum in Figure 6 was obtained at a 747.6 MHz ^{1}H NMR frequency with conditions that select signals from highly mobile residues in hydrated U-^{15}N,^{13}C-PrP fibrils, i.e., conditions similar to those in solution NMR experiments. The MAS frequency was only 5.25 kHz. ^{1}H decoupling in the t_2 period was accomplished with a continuous train of 25 μs π pulses, using a 25-element phase pattern generated by the [0,0,120,60,120] iterative scheme of Tycko et al. (*45*). ^{1}H evolution in the t_1 period occurred without homonuclear decoupling and with heteronuclear decoupling by a single ^{13}C π pulse at $t_1/2$. $^{1}H-^{13}C$ polarization transfer was accomplished with a refocused INEPT sequence (*46*), determined empirically to produce maximal ^{13}C NMR signals with a total mixing period of 3.6 ms. A total of 384 scans was acquired for each complex t_1 point, with 110 t_1 points and a 1.5 s recycle delay.

With the exception of Figure 6, ^{13}C chemical shifts are relative to tetramethylsilane (TMS), based on an external [1-^{13}C]alanine powder reference at 177.95 ppm. ^{15}N chemical shifts are relative to liquid NH_3, calculated using reported NMR frequency ratios (*47*).

Solid State NMR Data Analysis. Simulations of PITHIRDS-CT signals were performed with custom Fortran programs as previously described (*34*). Simulations without transverse (T_2) spin relaxation in Figure 1c used a five-spin system, with polarization initially on the central spin to minimize end effects and approximate the behavior of an infinite chain of spins. Simulations of the effects of T_2 relaxation in Figure 1d used a three-spin system and included continuous dephasing of coherences in the spin density matrix (using a direct-product basis), with dephasing rates equal to n_{qr}/T_2, where n_{qr} is the number of nuclear spins that change state in the coherence between basis state $|q>$ and basis state $|r>$ and T_2 is the transverse spin relaxation time.

2D NMR spectra of U-^{15}N,^{13}C-PrP fibrils were processed with NMRPipe (*48*) and analyzed and plotted with Sparky (http://www.cgl.ucsf.edu/home/sparky/). As recently described (*39*), site-specific assignments were generated from tables of $^{15}N-^{13}C_\alpha$ cross-peak chemical shifts, uncertainties, and degeneracies with a Monte Carlo/simulated annealing (MC/SA) algorithm in the program MCASSIGN1 (available upon request from robertty@mail.nih.gov). These tables are included in the Supporting Information (Tables S1 and S2). The cross-peak tables include residue-type assignments, which are allowed to be ambiguous whenever the data do not allow definite assignment of a $^{15}N-^{13}C_\alpha$ cross-peak to one residue type. The MC/SA algorithm assigns cross-peak signals to specific sites, consistent with information in the cross-peak tables, to maximize the score $S \equiv w_1N_g - w_2(N_b + N_e/4) - w_3N_u$. N_g and N_b are the numbers of "good connections" and "bad connections", respectively, meaning pairs of sequentially assigned NCOCX and NCACX cross-peaks with consistent and inconsistent chemical shifts as described previously (*39*); N_e is the number of assignment "edges", meaning dangling ends of sequentially assigned segments. N_u is the number of unassigned cross-peaks. In each MCASSIGN1 run, the parameters w_1 and w_2 were gradually incremented from 0 to 10 while assignment attempts were made. In this case, w_3 was always 0, so that unassigned cross-peaks were not directly penalized (although good connections were rewarded and edges were penalized). Each run used 1.5×10^8 attempts and required roughly 250 s on an Acer TravelMate 6292 computer; 100 independent runs were executed, 98 of which ended with $N_b = 0$ (i.e., no inconsistencies in the final site-specific ^{15}N and $^{13}C_\alpha$ chemical shifts). Final values of N_u were less than 5. Final scores ranged from 550 to 610.

The MC/SA algorithm is particularly well suited for data of the type reported below for U-^{15}N,^{13}C-PrP fibrils, in which

residue-type assignments in NCACX and NCOCX spectra are highly ambiguous because of low resolution and signal-to-noise ratio, and in which the number of cross-peaks is much smaller than the number of residues in the protein sequence. Manual sequential assignments are impossible in this case, because the information content of the data is insufficient for the determination of unique assignments. The MC/SA algorithm allows all assignments that are consistent with the available data to be identified. Examination of the complete set of possible assignments allows one to determine which residues have unique assignments, which residues definitely contribute to the solid state NMR spectra (and are therefore structurally ordered and relatively immobile), and which residues do not contribute to the solid state NMR spectra (and are therefore disordered and relatively dynamic). The MC/SA algorithm has been validated in experiments on uniformly ^{15}N- and ^{13}C-labeled HET-s$_{218-289}$ fibrils (*39*).

RESULTS

Intermolecular $^{13}C-^{13}C$ Dipole−Dipole Couplings Support a Parallel β-Sheet Structure. As previously demonstrated, the organization of β-sheets within amyloid fibrils can be determined with measurements of intermolecular dipole−dipole couplings among ^{13}C labels (*6*, *7*, *31*, *35*, *36*, *40*, *49*−*57*). An in-register parallel β-sheet structure leads to intermolecular $^{13}C-^{13}C$ distances of approximately 4.8 Å, the typical interstrand spacing in a β-sheet. At this distance, $^{13}C-^{13}C$ dipole−dipole couplings are approximately 70 Hz, leading to decays of ^{13}C NMR signals on the time scale of 30 ms when appropriate dipolar recoupling techniques are employed (*34*). Out-of-register or antiparallel β-sheets lead to longer $^{13}C-^{13}C$ distances and weaker couplings (proportional to the inverse cube of the distance) (*38*, *58*, *59*). Analogous experiments have also been performed with electron spins (*60*). When amyloid-forming polypeptides can be chemically synthesized, the ^{13}C labels can be introduced at a single site in each polypeptide chain, so that the measured couplings have a unique structural assignment (*6*, *7*, *38*, *40*, *49*, *51*−*55*, *61*). In the case of larger proteins such as PrP, single-site labeling is generally not possible. However, studies of yeast prion fibrils have shown that similar information can be obtained if the protein is ^{13}C-labeled biosynthetically at backbone carbonyl or side chain methyl sites of residues that occur multiple times but are well separated in the amino acid sequence (*31*, *35*, *36*, *56*, *57*). In such cases, the solid state NMR data reflect the intermolecular couplings of all labeled residues simultaneously. If some, but not all, labeled residues participate in the in-register parallel β-sheet structure, then a combination of rapidly decaying and slowly decaying signals may be observed (*57*).

Figure 1a shows measurements of $^{13}C-^{13}C$ dipole−dipole couplings in lyophilized ^{13}CO-F-PrP and ^{13}CO-I-PrP fibrils obtained with the PITHIRDS-CT dipolar recoupling technique (*34*). These are measurements of the dependence of the total carbonyl ^{13}C NMR signal on the effective recoupling period (i.e., the period of the PITHIRDS-CT pulse sequence during which $^{13}C-^{13}C$ couplings are active). Given the 1.1% natural abundance of ^{13}C and the large number of unlabeled carbonyl sites, approximately 48% of the total signal from ^{13}CO-F-PrP fibrils and approximately 41% of the total signal from ^{13}CO-I-PrP fibrils arise from natural-abundance ^{13}C sites, most of which are not coupled significantly to other ^{13}C nuclei. Therefore, Figure 1b shows the same PITHIRDS-CT data after subtraction of the expected natural-abundance signals, which are assumed to decay

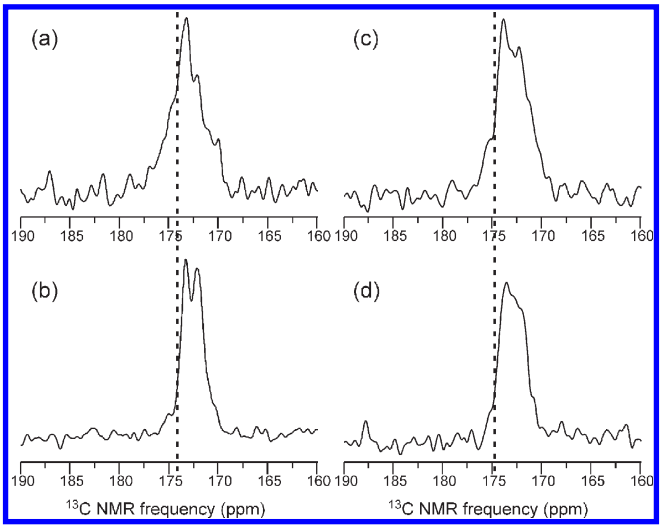

FIGURE 2: Solid state ^{13}C NMR spectra of ^{13}CO-F-PrP (a and b) and ^{13}CO-I-PrP (c and d) fibrils in the dry, lyophilized state (a and c) and after rehydration via addition of 3 μL of H_2O (b and d). Spectra were recorded at a 100.4 MHz ^{13}C NMR frequency with 20.00 kHz MAS and 368 (a) or 4096 (b−d) scans. Vertical dashed lines indicate the random-coil chemical shift values for F or I carbonyl sites.

linearly with increasing recoupling time to 70% of their initial value [as observed in earlier studies of yeast prion fibrils (*57*) and verified by PITHIRDS-CT measurements on PrP fibrils with a 1:4 dilution of ^{13}CO-I-PrP in unlabeled PrP]. The corrected data (and the raw data) show a decay on the 30 ms time scale, followed by a plateau at approximately 30% of the initial value for ^{13}CO-F-PrP fibrils, or approximately 10% of the initial value for ^{13}CO-I-PrP fibrils. Comparison with simulated PITHIRDS-CT data for an ideal linear chain of ^{13}C nuclei, shown in Figure 1c, indicates $^{13}C-^{13}C$ distances of 5.0−5.5 Å. While the ideal simulated data for a 5.0 Å distance show oscillations at recoupling times beyond 30 ms that are not present in the experimental data, the simulations in Figure 1d show that these oscillations are damped by transverse spin relaxation when $T_2 < 200$ ms. Actual T_2 values for backbone ^{13}CO sites under our experimental PITHIRDS-CT conditions are typically 50−100 ms. Thus, we conclude that the data in Figure 1a imply intermolecular $^{13}C-^{13}C$ distances of approximately 5.0 Å. Data for rehydrated samples, which agree with the data in Figure 1a but were acquired only to a maximum recoupling period of 38.4 ms, are shown in Figure S2 of the Supporting Information.

The most likely interpretation of these data is that the C-terminal half of PrP, which contains the three Phe and four Ile residues, forms in-register parallel β-sheets in PrP fibrils. The difference between the asymptotic values of ^{13}CO-F-PrP and ^{13}CO-I-PrP data suggests that one of the Phe residues (perhaps F141) may be outside the β-sheets. However, the asymptotic value of the corrected ^{13}CO-F-PrP data is not much higher than corresponding values in the linear chain simulations, and there is at least 10% uncertainty in the natural-abundance corrections. Relatively weak intramolecular dipole−dipole couplings between carbonyls of I182 and I184 and between carbonyls of I203 and I205 (6.5−7.0 Å distances in a β-strand) may also contribute to the lower asymptotic value of the ^{13}CO-I-PrP data. Therefore, we conclude that at least two (and possibly all three) Phe residues and all four Ile residues participate in the parallel β-sheet structure.

One-dimensional ^{13}C NMR spectra of the ^{13}CO-F-PrP and ^{13}CO-I-PrP fibril samples are shown in Figure 2. Relatively broad

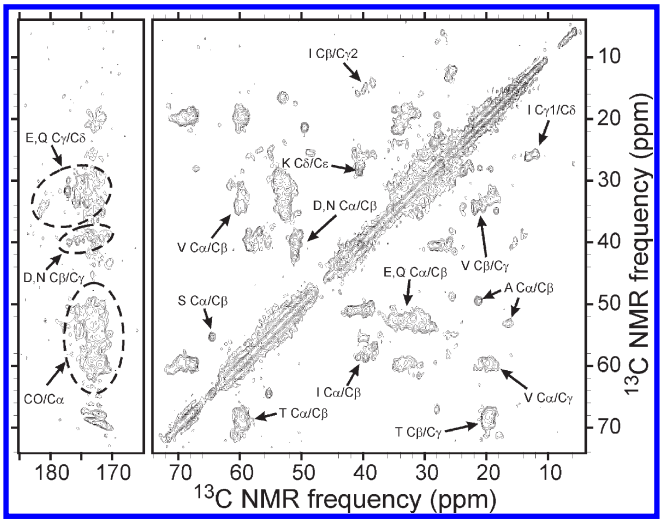

FIGURE 3: 2D $^{13}C-^{13}C$ solid state NMR spectrum of U-^{15}N,^{13}C-PrP fibrils. Partial residue-type assignments are shown for certain clusters of cross-peak signals.

carbonyl ^{13}C NMR lines [4 ppm full width at half-maximum (fwhm)] are observed in the dry, lyophilized state (Figure 2). Rehydration in the MAS rotor reduces the total carbonyl signal intensities by factors of 0.46 and 0.71 for ^{13}CO-F-PrP and ^{13}CO-I-PrP fibrils, respectively, and also reduces the line widths. These effects are due at least in part to elimination of natural-abundance signals from residues that are highly mobile in the hydrated state, i.e., residues that are outside of the β-sheet core. In the hydrated state, all carbonyl signals are shifted upfield relative to random-coil chemical shift values for Phe and Ile, consistent with β-strand conformations at the ^{13}C-labeled sites. For ^{13}CO-F-PrP, signals at 173.4 and 172.1 ppm are resolved in the hydrated state, with an area ratio of approximately 5:8. These signals may arise from one and two labeled Phe sites, respectively.

Identification of the Core-Forming Segment in PrP_{23-231} Fibrils. Solid state NMR measurements were performed on U-^{15}N,^{13}C-PrP fibrils in the hydrated state, with the goals of identifying the segment or segments of the PrP_{23-231} sequence that form the rigid core structure and characterizing the secondary structure within the core. Figure 3 shows a 2D $^{13}C-^{13}C$ spectrum of these fibrils in which cross-peaks arise primarily from one-bond, intraresidue spin polarization transfers. Several features are noteworthy. (i) Strong CO/C_α signals from Gly residues are not observed, although the PrP_{23-231} sequence contains 41 Gly residues. Such signals would be expected around 170 ppm/45 ppm. (ii) One Ser $C_\alpha-C_\beta$ cross-peak and two Ala $C_\alpha-C_\beta$ cross-peaks are observed, although the sequence contains seven Ser residues and eight Ala residues. (iii) At least three sets of Ile cross-peaks are observed. (iv) Signals from approximately five Val residues are observed, of the nine Val residues in the sequence. (v) Signals from eight or more Thr residues are observed, although they are not resolved from one another. (vi) Strong signals attributable to Pro residues are not observed. Taken together with the PrP_{23-231} sequence in Figure 1, these observations indicate that the core structure is composed primarily of residues in the 130−231 range.

To identify the segments that contribute to solid state NMR signals more precisely, we recorded the 2D $^{15}N-^{13}C$ spectra shown in Figure 4 and attempted to make sequential, site-specific resonance assignments. In favorable cases, assignments of signals from uniformly ^{15}N- and ^{13}C-labeled proteins can be made from such spectra via comparison of NCACX cross-peaks (Figure 4a), which link backbone ^{15}N chemical shifts with C_α and side chain ^{13}C chemical shifts within individual residues, with NCOCX cross-peaks (Figure 4c), which link the backbone ^{15}N chemical shift of a given residue with ^{13}C chemical shifts of the preceding residue in the amino acid sequence. If the cross-peaks are sufficiently well-resolved and if many cross-peaks can be assigned to residue types based on their characteristic ^{13}C chemical shift ranges (*62*), then site-specific assignments can be made manually. Unfortunately, the 2D spectra in Figures 3 and 4 are only partially resolved (full width at half-maximum line widths of approximately 0.5−0.8 and 1.0−1.3 ppm for ^{13}C and ^{15}N NMR signals, respectively), and only a small number of $N-C_\beta$ cross-peaks could be detected above the noise level, making residue-type assignments difficult. Therefore, manual sequential assignments could not be made uniquely. Instead, we used a computational approach to enumerate possible assignments that are consistent with the detected cross-peaks (*39*). In this approach, the program MCASSIGN1 is provided with input tables containing chemical shifts of $N-C_\alpha$ cross-peaks from NCACX and NCOCX spectra, uncertainties in the shifts, cross-peak degeneracies (in case more than one $N-C_\alpha$ pair contributes to a single cross-peak), and possible residue-type assignments. MCASSIGN1 then uses a MC/SA algorithm to find site-specific assignments that are consistent with these inputs. In principle, multiple independent runs allow all consistent assignments to be identified.

Cross-peak tables for the spectra in Figure 4 are given in the Supporting Information (Tables S1 and S2). Residue-type assignments in these tables (also shown in Figure 4a,c) were made primarily by comparing $^{13}C_\alpha$ chemical shifts in the NCACX and NCOCX spectra with cross-peak positions in the 2D $^{13}C-^{13}C$ spectrum. For many of the cross-peaks, residue-type assignments were highly ambiguous. One hundred MCASSIGN1 runs yielded 98 consistent assignments (not all different from one another). The highest-scoring assignment (score of 610; see Materials and Methods) is shown in panels b and d of Figure 4.

The cross-peak tables allow only 36 residues to be assigned to NCACX cross-peaks and 35 residues to be assigned to NCOCX cross-peaks, limited by the number of definite cross-peaks in each 2D spectrum and their apparent degeneracies. The identities of residues in the PrP_{23-231} sequence that occurred in the final assignment varied significantly among the MCASSIGN1 runs. Panels a and b of Figure 5 show the fractions of successful runs in which each residue was assigned to NCACX and NCOCX cross-peaks. These plots can be interpreted loosely as indications of the probability that a given residue contributes to the solid state NMR signals, i.e., participates in the rigid core of PrP_{23-231} fibrils. The core structure is comprised primarily of residues in the 173−224 range, but we cannot rule out participation of certain segments in the 95−161 range (including F141). For example, Figure 3 shows two $C_\alpha-C_\beta$ cross-peaks from Ala residues, while Figure 5 suggests that these cross-peaks arise from A224 and A120.

The 2D $^{13}C-^{13}C$ spectrum in Figure 3 shows a single Ser $C_\alpha-C_\beta$ cross-peak (apparently S222) with β-strand-like chemical shifts (upfield relative to the random-coil value for C_α, downfield for C_β). All Ile $C_\alpha-C_\beta$ cross-peak signals are also β-strand-like. $C_\alpha-C_\beta$ cross-peak signals for Thr and Val are primarily at β-strand-like chemical shifts, but several Thr residues (of 14 in PrP_{23-231}) and at least one Val residue (of nine) apparently contribute signals with non-β-strand shifts. [For these comparisons,

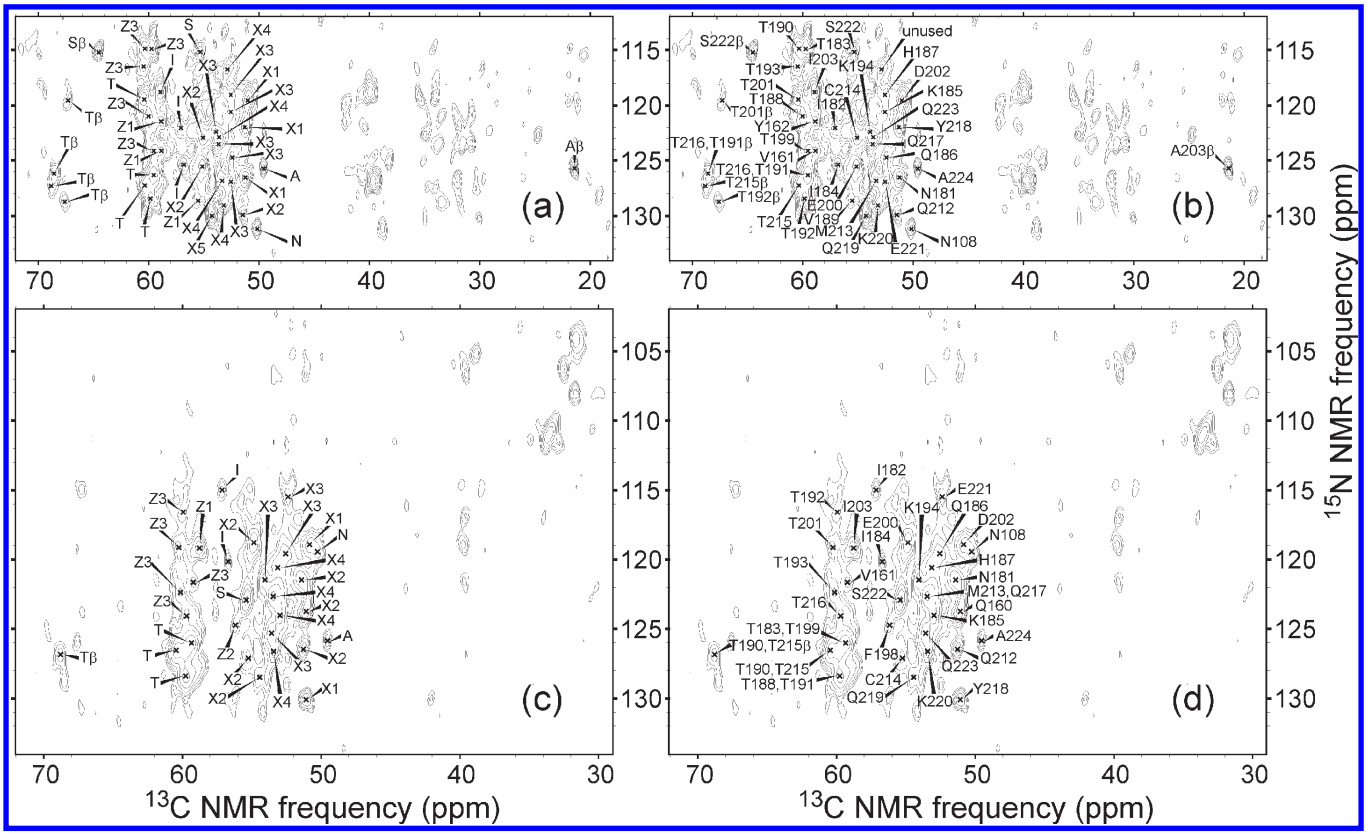

FIGURE 4: 2D ^{15}N−^{13}C solid state NMR spectra of U-^{15}N,^{13}C-PrP fibrils, including the NCACX spectrum (a and b) and the NCOCX spectrum (c and d). Residue-type assignments for N−C$_\alpha$ cross-peaks that are used for automated site-specific assignments are shown in panels a and c, with the following definitions for ambiguous residue-type assignments: X1, CDLNFY; X2, CDEFHKLMNQRWY; X3, EHKMQRW; X4, EHKMQRWA; X5, CEHKMQRW; Z1, IFYLV; Z2, IFYL; Z3, VT. Several N−C$_\beta$ cross-peaks are also indicated, for example, by Tβ. Possible site-specific assignments of the same cross-peaks are shown in panels b and d. These are the highest-scoring assignments, as explained in the text, but are not unique.

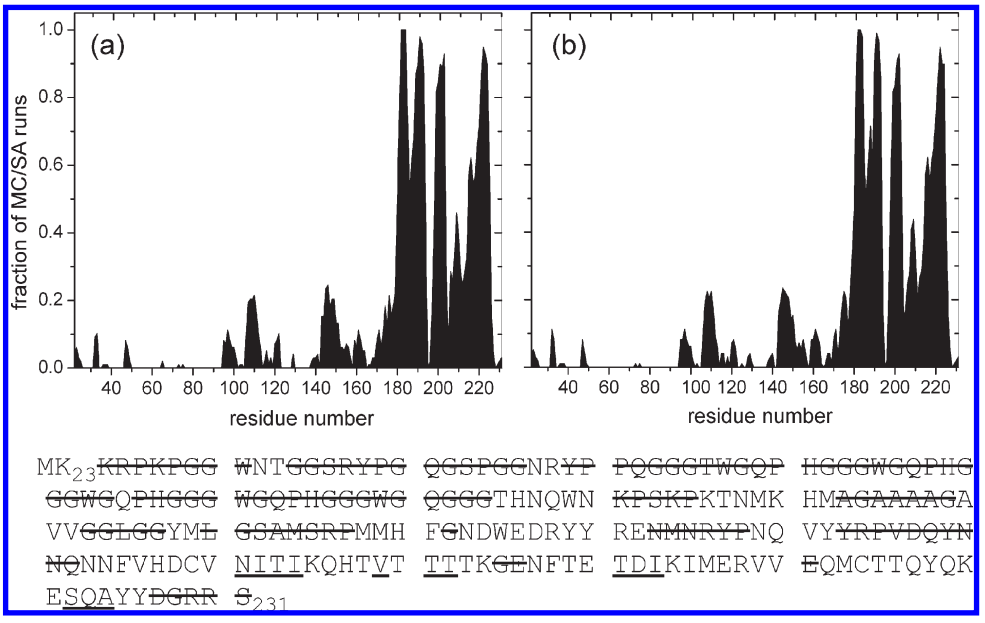

FIGURE 5: Summary of the results of automated site-specific assignments for U-^{15}N,^{13}C-PrP fibrils, using the spectra in Figures 3 and 4. Graphs show the fraction of MC/SA assignment runs in which each residue has assigned signals in the NCACX (a) and NCOCX (b) spectrum. In the 11 highest-scoring assignments, residues that never have assigned signals in either spectrum are struck through in the PrP sequence below the graphs; residues that always have assigned signals in at least one spectrum are underlined.

random-coil shifts reported by Wishart et al. (*62*) are used, adjusted to our TMS reference by subtraction of 1.7 ppm.]

Several residues have unique NCACX assignments (and are always assigned) in the 11 highest-scoring MCASSIGN1 runs, namely, I182, T183, I184, I203, S222, Q223, and A224. For all of these residues, the ^{13}C$_\alpha$ chemical shifts in the NCACX spectrum are upfield of random-coil values, consistent with β-strand secondary structure. V189 and T192 are also always assigned

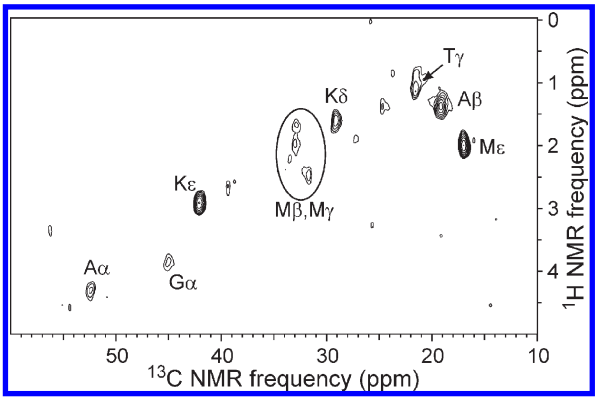

FIGURE 6: 2D ^{1}H−^{13}C NMR spectrum of U-^{15}N,^{13}C-PrP fibrils, obtained under conditions that select signals from highly mobile residues (see the text). Assignments to sites on certain residue types are based on reported random-coil chemical shifts (*62*). Chemical shift scales are relative to 2,2-dimethyl-2-silapentane 5-sulfonate.

(but not uniquely) in the 11 highest-scoring runs, with only β-strand-like $^{13}C_\alpha$ chemical shifts. No residues are consistently assigned with non-β-strand $^{13}C_\alpha$ chemical shifts. Thus, the MCASSIGN1 analysis indicates that residues 182−184 and 222−224 are most likely in β-strands. Current data do not permit us to draw conclusions regarding the length of these β-strands or the location of non-β-strand segments that may connect the β-strands.

MCASSIGN1 runs were also executed with the assumption that only residues 160−231 contribute to the solid state NMR spectra. Assignments with scores as high as 610 were obtained, but the assignments were not more unique than when the full PrP_{23-231} sequence was included.

Additional information about the identities of rigid and mobile residues comes from spectra obtained under conditions appropriate for solution NMR (rather than solid state NMR). Figure 6 shows a 2D ^{1}H−^{13}C spectrum obtained under such conditions. Signals that can be assigned to Ala, Gly, Lys, Met, and Thr residues are observed, with assignments based on random-coil shifts (*62*). All of these residues occur at multiple positions in the N-terminal half of the PrP_{23-231} sequence. However, the observation of relatively weak Gly signals, despite the fact that Gly accounts for 35% of residues from positions 23 to 131, indicates that the N-terminal half is not as mobile as a fully disordered polypeptide in solution [e.g., monomeric α-synuclein (*63*)] or as in monomeric PrP_{23-231}, which exhibits subnanosecond orientational correlation times, minimal chemical shift dispersion, and negative ^{1}H−^{15}N nuclear Overhauser effects for residues 23−120 in solution NMR measurements (*28*, *29*). Steric restrictions or transient population of ordered structures may affect the time scale and amplitude of N-terminal motions, leading to relatively short T_2 times and hence weak signals under the experimental conditions described in the legend of Figure 6. Alternatively, the N-terminal half may contain a mixture of immobile and mobile segments in the fibrillar state. Recent evidence that N-terminal residues influence PrP_{23-231} fibril morphology may be relevant to our observation of restricted mobility for the N-terminal half (*64*).

DISCUSSION

In monomeric PrP_{23-231}, residues 144−156, 172−193, and 200−227 form α-helices (*29*). The data presented above indicate that a large part of these helical segments, most likely including most of the second and third helical segments, undergoes a major conformational change to form the amyloid fibril core in the recombinant PrP_{23-231} fibrils studied in this work. The β-sheets in these fibrils have the in-register parallel structure observed previously in several other amyloid fibrils (*6*, *18*, *20*, *31*, *36*, *52*, *57*, *65*, *66*). Although the precise location of β-strands cannot be determined from our data, the analysis presented above indicates that the fibril core is most likely formed by residues in the 173−224 range, with residues 182−184 and 222−224 being part of β-strands.

These results from solid state NMR are consistent with previous studies in which proteinase K (PK) digestion, immunofluorescence microscopy, and site-specific conformational stability assays were employed to assess the structure of fibrils produced in vitro from full-length PrP (*67*−*69*). The PK-resistant fragments of the amyloid fibrils were found to consist of residues 138/141−230, 152/153−230, and 162−230, with residues 162−230 being was the most resistant to proteolytic treatment (*13*, *70*). Upon treatment with PK, the fragments of residues 152/153−230 and 162−230 preserved a high β-sheet content, a fibrillar appearance, and high seeding activity in fibrillation assays (*13*), supporting the notion that the cross-β core is formed within residues 162−230. Our solid state NMR data indicate that less than 25% of the full-length PrP sequence acquires a β-strand conformation in the amyloid fibrils. This result is consistent with a relatively low level of amide hydrogen protection measured by H−D exchange FTIR spectroscopy (*27*). Despite the small fraction of residues that adopt β-sheet conformations, PrP fibrils exhibit remarkably high conformational stability, with a GdnHCl denaturation midpoint above 4 M (*67*). This observation suggests that, in addition to hydrogen bonds, hydrophobic and electrostatic interactions contribute substantially to the conformational stability of PrP fibrils.

Our results are also consistent with the findings of Surewicz and co-workers, who obtained evidence from H−D exchange measurements that the second and third helical segments of human PrP_{90-231} form the core structure in amyloid fibrils prepared in vitro (*24*) and used EPR spectroscopy of spin-labeled samples to show that approximately residues 160−220 form an in-register parallel β-sheet structure (*25*). The agreement between our results and these earlier findings is remarkable in light of the fact that our PrP sequence is different, our fibril formation protocol is different, and our experimental measurements are different. An in-register parallel β-sheet core formed by the C-terminal portion may be a general feature of recombinant PrP fibrils formed in vitro.

Solid state NMR measurements on PrP_{23-144} fibrils indicate that the structured core consists of residues 112−141 (*15*, *19*). According to Figure 5, most of this segment is not included in the core of our PrP_{23-231} fibrils. For example, the AGAAAAGA segment (residues 113−120) does not contribute to the 2D ^{13}C−^{13}C spectrum in Figure 3, which shows only two C_α−C_β cross-peaks from Ala residues and no strong CO−C_α cross-peaks from Gly residues. Previous biophysical measurements also indicate that this segment is solvent-expposed or unstructured in recombinant PrP_{23-231} fibrils (*67*−*69*).

The molecular structures of PrP fibrils formed in vitro may be significantly different from those of infectious PrP^{Sc} strains. For example, Wille et al. have shown that infectious PrP(27−30) rods produce X-ray fiber diffraction patterns different from those of recombinant fibrils (*71*), although both materials show the 4.8 Å

meridional diffraction feature that is characteristic of a cross-β structure and both have the appearance of amyloid fibrils in EM images. The protease-resistant core of PrP^{Sc} also extends further toward the N-terminus than does the protease-resistant core of recombinant PrP fibrils (*68*, *70*, *72*). Therefore, our results do not necessarily apply to PrP^{Sc}.

While recombinant PrP fibrils and PrP^{Sc} may have different overall structures, they appear to share some common structural elements, as is evident from similarities in PK digestion patterns performed under partially denaturing conditions (*68*, *73*). Furthermore, transmissible prion diseases have been induced in wild-type animals by inoculation with recombinant PrP fibril preparations produced in vitro (*72*, *74*), indicating that at least one component of these preparations structurally resembles PrP^{Sc} or is capable of converting to PrP^{Sc} (or catalyzing PrP^{Sc} formation) in the biological environment. We speculate that partial structural similarities between recombinant PrP fibrils and PrP^{Sc} may be sufficient to produce transmissible prion disease. Therefore, while recombinant PrP fibrils have limited infectivity, knowledge of their structures together with that of PrP^{Sc} is important for elucidating the molecular mechanisms responsible for the genesis and evolution of infectious prions.

An in-register parallel β-sheet structure formed by residues 173−224 is fundamentally different from the β-helical model for PrP^{Sc} proposed by Govaerts et al. (*75*), in which residues 89−174 form a left-handed β-helical structure and the second and third α-helices of monomeric PrP are retained. While the current solid state NMR results for PrP_{23-231} fibrils cannot be used to judge whether the β-helical model of PrP^{Sc} is correct, previous studies argue that residues 90−140 are less likely to form the core structure in PrP^{Sc}. Antibodies specific to residues 90−110 were found to precipitate native PrP^{Sc}, arguing that this region is exposed to the solvent to an extent sufficient for immunoprecipitation (*76*). Furthermore, incubation of PrP^{Sc} with 2−3 M GdnHCl was shown to destabilize the central region (residues 90−140), which had acquired a PK-sensitive conformation, while the C-terminal part (residues 143−230) remained PK-resistant (*77*).

SUPPORTING INFORMATION AVAILABLE

Figures S1 and S2 showing EM and AFM images of isotopically labeled PrP_{23-231} fibrils and PITHIRDS-CT data for fibrils after rehydration, respectively, and Tables S1 and S2 containing the input to MCASSIGN1 for automated assignment of NCACX and NCOCX cross-peaks. This material is available free of charge via the Internet at http://pubs.acs.org.

REFERENCES

1. Prusiner, S. B. (1998) Prions. *Proc. Natl. Acad. Sci. U.S.A. 95*, 13363–13383.
2. Silveira, J. R., Raymond, G. J., Hughson, A. G., Race, R. E., Sim, V. L., Hayes, S. F., and Caughey, B. (2005) The most infectious prion protein particles. *Nature 437*, 257–261.
3. Tycko, R. (2006) Molecular structure of amyloid fibrils: Insights from solid state NMR. *Q. Rev. Biophys. 39*, 1–55.
4. Safar, J., Wille, H., Itrri, V., Groth, D., Serban, H., Torchia, M., Cohen, F. E., and Prusiner, S. B. (1998) Eight prion strains have PrP^{Sc} molecules with different conformations. *Nat. Med. 4*, 1157–1165.
5. Bessen, R. A., Kocisko, D. A., Raymond, G. J., Nandan, S., Lansbury, P. T., and Caughey, B. (1995) Nongenetic propagation of strain-specific properties of scrapie prion protein. *Nature 375*, 698–700.
6. Paravastu, A. K., Leapman, R. D., Yau, W. M., and Tycko, R. (2008) Molecular structural basis for polymorphism in Alzheimer's β-amyloid fibrils. *Proc. Natl. Acad. Sci. U.S.A. 105*, 18349–18354.
7. Petkova, A. T., Leapman, R. D., Guo, Z. H., Yau, W. M., Mattson, M. P., and Tycko, R. (2005) Self-propagating, molecular-level polymorphism in Alzheimer's β-amyloid fibrils. *Science 307*, 262–265.
8. Edskes, H. K., McCann, L. M., Hebert, A. M., and Wickner, R. B. (2009) Prion variants and species barriers among *Saccharomyces* ure2 proteins. *Genetics 181*, 1159–1167.
9. Toyama, B. H., Kelly, M. J. S., Gross, J. D., and Weissman, J. S. (2007) The structural basis of yeast prion strain variants. *Nature 449*, 233–237.
10. King, C. Y., and Diaz-Avalos, R. (2004) Protein-only transmission of three yeast prion strains. *Nature 428*, 319–323.
11. Derkatch, I. L., Chernoff, Y. O., Kushnirov, V. V., Inge-Vechtomov, S. G., and Liebman, S. W. (1996) Genesis and variability of [PSI] prion factors in *Saccharomyces cerevisiae*. *Genetics 144*, 1375–1386.
12. Swietnicki, W., Morillas, M., Chen, S. G., Gambetti, P., and Surewicz, W. K. (2000) Aggregation and fibrillization of the recombinant human prion protein $huPrP_{90-231}$. *Biochemistry 39*, 424–431.
13. Bocharova, O. V., Breydo, L., Parfenov, A. S., Salnikov, V. V., and Baskakov, I. V. (2005) In vitro conversion of full-length mammalian prion protein produces amyloid form with physical properties of PrP^{Sc}. *J. Mol. Biol. 346*, 645–659.
14. Lim, K. H., Nguyen, T. N., Damo, S. M., Mazur, T., Ball, H. L., Prusiner, S. B., Pines, A., and Wemmer, D. E. (2006) Solid state NMR structural studies of the fibril form of a mutant mouse prion peptide PrP_{89-143}. *Solid State Nucl. Magn. Reson. 29*, 183–190.
15. Helmus, J. J., Surewicz, K., Nadaud, P. S., Surewicz, W. K., and Jaroniec, C. P. (2008) Molecular conformation and dynamics of the Y145Stop variant of human prion protein. *Proc. Natl. Acad. Sci. U.S.A. 105*, 6284–6289.
16. Lee, S. W., Mou, Y., Lin, S. Y., Chou, F. C., Tseng, W. H., Chen, C., Lu, C. Y. D., Yu, S. S. F., and Chan, J. C. C. (2008) Steric zipper of the amyloid fibrils formed by residues 109−122 of the Syrian hamster prion protein. *J. Mol. Biol. 378*, 1142–1154.
17. Makarava, N., and Baskakov, I. V. (2008) The same primary structure of the prion protein yields two distinct self-propagating states. *J. Biol. Chem. 283*, 15988–15996.
18. Walsh, P., Simonetti, K., and Sharpe, S. (2009) Core structure of amyloid fibrils formed by residues 106−126 of the human prion protein. *Structure 17*, 417–426.
19. Helmus, J. J., Surewicz, K., Surewicz, W. K., and Jaroniec, C. P. (2010) Conformational flexibility of Y145Stop human prion protein amyloid fibrils probed by solid state nuclear magnetic resonance spectroscopy. *J. Am. Chem. Soc. 132*, 2393–2403.
20. Lin, N. S., Chao, J. C. H., Cheng, H. M., Chou, F. C., Chang, C. F., Chen, Y. R., Chang, Y. J., Huang, S. J., and Chan, J. C. C. (2010) Molecular structure of amyloid fibrils formed by residues 127 to 147 of the human prion protein. *Chem.—Eur. J. 16*, 5492–5499.
21. Novitskaya, V., Bocharova, O. V., Bronstein, I., and Baskakov, I. V. (2006) Amyloid fibrils of mammalian prion protein are highly toxic to cultured cells and primary neurons. *J. Biol. Chem. 281*, 13828–13836.
22. Kundu, B., Maiti, N. R., Jones, E. M., Surewicz, K. A., Vanik, D. L., and Surewicz, W. K. (2003) Nucleation-dependent conformational conversion of the Y145Stop variant of human prion protein: Structural clues for prion propagation. *Proc. Natl. Acad. Sci. U.S.A. 100*, 12069–12074.
23. Sun, Y., Makarava, N., Lee, C. I., Laksanalamai, P., Robb, F. T., and Baskakov, I. V. (2008) Conformational stability of PrP amyloid fibrils controls their smallest possible fragment size. *J. Mol. Biol. 376*, 1155–1167.
24. Lu, X. J., Wintrode, P. L., and Surewicz, W. K. (2007) β-Sheet core of human prion protein amyloid fibrils as determined by hydrogen/deuterium exchange. *Proc. Natl. Acad. Sci. U.S.A. 104*, 1510–1515.
25. Cobb, N. J., Sonnichsen, F. D., McHaourab, H., and Surewicz, W. K. (2007) Molecular architecture of human prion protein amyloid: A parallel, in-register β-structure. *Proc. Natl. Acad. Sci. U.S.A. 104*, 18946–18951.
26. Jones, E. M., Surewicz, K., and Surewicz, W. K. (2006) Role of N-terminal familial mutations in prion protein fibrillization and prion amyloid propagation in vitro. *J. Biol. Chem. 281*, 8190–8196.
27. Ostapchenko, V. G., Sawaya, M. R., Makarava, N., Savtchenko, R., Nilsson, K. P. R., Eisenberg, D., and Baskakov, I. V. (2010) Two amyloid states of the prion protein display signficantly different folding patterns. *J. Mol. Biol. 400*, 908–921.
28. Riek, R., Hornemann, S., Wider, G., Glockshuber, R., and Wuthrich, K. (1997) NMR characterization of the full-length recombinant murine prion protein, mPrP(23−231). *FEBS Lett. 413*, 282–288.
29. Donne, D. G., Viles, J. H., Groth, D., Mehlhorn, I., James, T. L., Cohen, F. E., Prusiner, S. B., Wright, P. E., and Dyson, H. J. (1997) Structure of the recombinant full-length hamster prion protein PrP_{29-231}: The N terminus is highly flexible. *Proc. Natl. Acad. Sci. U.S.A. 94*, 13452–13457.
30. Breydo, L., Bocharova, O. V., Makarava, N., Salnikov, V. V., Anderson, M., and Baskakov, I. V. (2005) Methionine oxidation

interferes with conversion of the prion protein into the fibrillar proteinase K-resistant conformation. *Biochemistry 44*, 15534–15543.
31. Baxa, U., Wickner, R. B., Steven, A. C., Anderson, D. E., Marekov, L. N., Yau, W. M., and Tycko, R. (2007) Characterization of β-sheet structure in Ure2p$_{1-89}$ yeast prion fibrils by solid state nuclear magnetic resonance. *Biochemistry 46*, 13149–13162.
32. Cai, M. L., Huang, Y., Sakaguchi, K., Clore, G. M., Gronenborn, A. M., and Craigie, R. (1998) An efficient and cost-effective isotope labeling protocol for proteins expressed in *Escherichia coli*. *J. Biomol. NMR 11*, 97–102.
33. Baskakov, I. V., and Bocharova, O. V. (2005) In vitro conversion of mammalian prion protein into amyloid fibrils displays unusual features. *Biochemistry 44*, 2339–2348.
34. Tycko, R. (2007) Symmetry-based constant-time homonuclear dipolar recoupling in solid state NMR. *J. Chem. Phys. 126*, 064506.
35. Shewmaker, F., Ross, E. D., Tycko, R., and Wickner, R. B. (2008) Amyloids of shuffled prion domains that form prions have a parallel in-register β-sheet structure. *Biochemistry 47*, 4000–4007.
36. Wickner, R. B., Dyda, F., and Tycko, R. (2008) Amyloid of Rnq1p, the basis of the [PIN+] prion, has a parallel in-register β-sheet structure. *Proc. Natl. Acad. Sci. U.S.A. 105*, 2403–2408.
37. Petkova, A. T., and Tycko, R. (2002) Sensitivity enhancement in structural measurements by solid state NMR through pulsed spin locking. *J. Magn. Reson. 155*, 293–299.
38. Petkova, A. T., Buntkowsky, G., Dyda, F., Leapman, R. D., Yau, W. M., and Tycko, R. (2004) Solid state NMR reveals a pH-dependent antiparallel β-sheet registry in fibrils formed by a β-amyloid peptide. *J. Mol. Biol. 335*, 247–260.
39. Tycko, R., and Hu, K.-N. (2010) A Monte Carlo/simulated annealing algorithm for sequential resonance assignment in solid state NMR of uniformly labeled proteins with magic-angle spinning. *J. Magn. Reson. 205*, 304–314.
40. Paravastu, A. K., Petkova, A. T., and Tycko, R. (2006) Polymorphic fibril formation by residues 10−40 of the Alzheimer's β-amyloid peptide. *Biophys. J. 90*, 4618–4629.
41. Bennett, A. E., Rienstra, C. M., Griffiths, J. M., Zhen, W. G., Lansbury, P. T., and Griffin, R. G. (1998) Homonuclear radio frequency-driven recoupling in rotating solids. *J. Chem. Phys. 108*, 9463–9479.
42. Ishii, Y. (2001) ^{13}C-^{13}C dipolar recoupling under very fast magic angle spinning in solid state nuclear magnetic resonance: Applications to distance measurements, spectral assignments, and high-throughput secondary-structure determination. *J. Chem. Phys. 114*, 8473–8483.
43. Bennett, A. E., Rienstra, C. M., Auger, M., Lakshmi, K. V., and Griffin, R. G. (1995) Heteronuclear decoupling in rotating solids. *J. Chem. Phys. 103*, 6951–6958.
44. Baldus, M., Petkova, A. T., Herzfeld, J., and Griffin, R. G. (1998) Cross polarization in the tilted frame: Assignment and spectral simplification in heteronuclear spin systems. *Mol. Phys. 95*, 1197–1207.
45. Tycko, R., Pines, A., and Guckenheimer, J. (1985) Fixed-point theory of iterative excitation schemes in NMR. *J. Chem. Phys. 83*, 2775–2802.
46. Morris, G. A., and Freeman, R. (1979) Enhancement of nuclear magnetic-resonance signals by polarization transfer. *J. Am. Chem. Soc. 101*, 760–762.
47. Wishart, D. S., Bigam, C. G., Yao, J., Abildgaard, F., Dyson, H. J., Oldfield, E., Markley, J. L., and Sykes, B. D. (1995) ^{1}H, ^{13}C, and ^{15}N chemical shift referencing in biomolecular NMR. *J. Biomol. NMR 6*, 135–140.
48. Delaglio, F., Grzesiek, S., Vuister, G. W., Zhu, G., Pfeifer, J., and Bax, A. (1995) NMRpipe: A multidimensional spectral processing system based on Unix pipes. *J. Biomol. NMR 6*, 277–293.
49. Benzinger, T. L. S., Gregory, D. M., Burkoth, T. S., Miller-Auer, H., Lynn, D. G., Botto, R. E., and Meredith, S. C. (1998) Propagating structure of Alzheimer's β-amyloid(10−35) is parallel β-sheet with residues in exact register. *Proc. Natl. Acad. Sci. U.S.A. 95*, 13407–13412.
50. Gregory, D. M., Benzinger, T. L. S., Burkoth, T. S., Miller-Auer, H., Lynn, D. G., Meredith, S. C., and Botto, R. E. (1998) Dipolar recoupling NMR of biomolecular self-assemblies: Determining inter- and intrastrand distances in fibrilized Alzheimer's β-amyloid peptide. *Solid State Nucl. Magn. Reson. 13*, 149–166.
51. Antzutkin, O. N., Balbach, J. J., Leapman, R. D., Rizzo, N. W., Reed, J., and Tycko, R. (2000) Multiple quantum solid state NMR indicates a parallel, not antiparallel, organization of β-sheets in Alzheimer's β-amyloid fibrils. *Proc. Natl. Acad. Sci. U.S.A. 97*, 13045–13050.
52. Antzutkin, O. N., Leapman, R. D., Balbach, J. J., and Tycko, R. (2002) Supramolecular structural constraints on Alzheimer's β-amyloid fibrils from electron microscopy and solid state nuclear magnetic resonance. *Biochemistry 41*, 15436–15450.
53. Balbach, J. J., Petkova, A. T., Oyler, N. A., Antzutkin, O. N., Gordon, D. J., Meredith, S. C., and Tycko, R. (2002) Supramolecular structure in full-length Alzheimer's β-amyloid fibrils: Evidence for a parallel β-sheet organization from solid state nuclear magnetic resonance. *Biophys. J. 83*, 1205–1216.
54. Chan, J. C. C., Oyler, N. A., Yau, W. M., and Tycko, R. (2005) Parallel β-sheets and polar zippers in amyloid fibrils formed by residues 10−39 of the yeast prion protein Ure2p. *Biochemistry 44*, 10669–10680.
55. Luca, S., Yau, W. M., Leapman, R., and Tycko, R. (2007) Peptide conformation and supramolecular organization in amylin fibrils: Constraints from solid state NMR. *Biochemistry 46*, 13505–13522.
56. Shewmaker, F., Kryndushkin, D., Chen, B., Tycko, R., and Wickner, R. B. (2009) Two prion variants of Sup35p have in-register parallel β-sheet structures, independent of hydration. *Biochemistry 48*, 5074–5082.
57. Shewmaker, F., Wickner, R. B., and Tycko, R. (2006) Amyloid of the prion domain of Sup35p has an in-register parallel β-sheet structure. *Proc. Natl. Acad. Sci. U.S.A. 103*, 19754–19759.
58. Tycko, R., Sciarretta, K. L., Orgel, J., and Meredith, S. C. (2009) Evidence for novel β-sheet structures in Iowa mutant β-amyloid fibrils. *Biochemistry 48*, 6072–6084.
59. Shewmaker, F., McGlinchey, R. P., Thurber, K. R., McPhie, P., Dyda, F., Tycko, R., and Wickner, R. B. (2009) The functional curli amyloid is not based on in-register parallel β-sheet structure. *J. Biol. Chem. 284*, 25065–25076.
60. Margittai, M., and Langen, R. (2008) Fibrils with parallel in-register structure constitute a major class of amyloid fibrils: Molecular insights from electron paramagnetic resonance spectroscopy. *Q. Rev. Biophys. 41*, 265–297.
61. Balbach, J. J., Ishii, Y., Antzutkin, O. N., Leapman, R. D., Rizzo, N. W., Dyda, F., Reed, J., and Tycko, R. (2000) Amyloid fibril formation by Aβ_{16-22}, a seven-residue fragment of the Alzheimer's β-amyloid peptide, and structural characterization by solid state NMR. *Biochemistry 39*, 13748–13759.
62. Wishart, D. S., Bigam, C. G., Holm, A., Hodges, R. S., and Sykes, B. D. (1995) ^{1}H, ^{13}C, and ^{15}N random coil NMR chemical shifts of the common amino acids: 1. Investigations of nearest-neighbor effects. *J. Biomol. NMR 5*, 67–81.
63. Wu, K. P., Kim, S., Fela, D. A., and Baum, J. (2008) Characterization of conformational and dynamic properties of natively unfolded human and mouse α-synuclein ensembles by NMR: Implication for aggregation. *J. Mol. Biol. 378*, 1104–1115.
64. Ostapchenko, V. G., Makarava, N., Savtchenko, R., and Baskakov, I. V. (2008) The polybasic N-terminal region of the prion protein controls the physical properties of both the cellular and fibrillar forms of PrP. *J. Mol. Biol. 383*, 1210–1224.
65. Ladner, C. L., Chen, M., Smith, D. P., Platt, G. W., Radford, S. E., and Langen, R. (2010) Stacked sets of parallel, in-register β-strands of β_2-microglobulin in amyloid fibrils revealed by site-directed spin labeling and chemical labeling. *J. Biol. Chem. 285*, 17137–17147.
66. Chen, M., Margittai, M., Chen, J., and Langen, R. (2007) Investigation of α-synuclein fibril structure by site-directed spin labeling. *J. Biol. Chem. 282*, 24970–24979.
67. Sun, Y., Breydo, L., Makarava, N., Yang, Q. Y., Bocharova, O. V., and Baskakov, I. V. (2007) Site-specific conformational studies of prion protein (PrP) amyloid fibrils revealed two cooperative folding domains within amyloid structure. *J. Biol. Chem. 282*, 9090–9097.
68. Bocharova, O. V., Breydo, L., Salnikov, V. V., Gill, A. C., and Baskakov, I. V. (2005) Synthetic prions generated in vitro are similar to a newly identified subpopulation of PrP^{Sc} from sporadic Creutzfeldt-Jakob disease. *Protein Sci. 14*, 1222–1232.
69. Novitskaya, V., Makarava, N., Bellon, A., Bocharova, O. V., Bronstein, I. B., Williamson, R. A., and Baskakov, I. V. (2006) Probing the conformation of the prion protein within a single amyloid fibril using a novel immunoconformational assay. *J. Biol. Chem. 281*, 15536–15545.
70. Bocharova, O. V., Makarava, N., Breydo, L., Anderson, M., Salnikov, V. V., and Baskakov, I. V. (2006) Annealing prion protein amyloid fibrils at high temperature results in extension of a proteinase K-resistant core. *J. Biol. Chem. 281*, 2373–2379.
71. Wille, H., Bian, W., McDonald, M., Kendall, A., Colby, D. W., Bloch, L., Ollesch, J., Borovinskiy, A. L., Cohen, F. E., Prusiner, S. B., and Stubbs, G. (2009) Natural and synthetic prion structure from X-ray fiber diffraction. *Proc. Natl. Acad. Sci. U.S.A. 106*, 16990–16995.

72. Makarava, N., Kovacs, G. G., Bocharova, O., Savtchenko, R., Alexeeva, I., Budka, H., Rohwer, R. G., and Baskakov, I. V. (2010) Recombinant prion protein induces a new transmissible prion disease in wild-type animals. *Acta Neuropathol. 119*, 177–187.
73. Sajnani, G., Pastrana, M. A., Dynin, I., Onisko, B., and Requena, J. R. (2008) Scrapie prion protein structural constraints obtained by limited proteolysis and mass spectrometry. *J. Mol. Biol. 382*, 88–98.
74. Wang, F., Wang, X., Yuan, C.-G., and Ma, J. (2010) Generating a prion with bacterially expressed recombinant prion. *Protein Sci. 327*, 1132–1135.
75. Govaerts, C., Wille, H., Prusiner, S. B., and Cohen, F. E. (2004) Evidence for assembly of prions with left-handed β-helices into trimers. *Proc. Natl. Acad. Sci. U.S.A. 101*, 8342–8347.
76. Khalili-Shirazi, A., Summers, L., Linehan, J., Mallinson, G., Anstee, D., Hawke, S., Jackson, G. S., and Collinge, J. (2005) PrP glycoforms are associated in a strain-specific ratio in native PrP^{Sc}. *J. Gen. Virol. 86*, 2635–2644.
77. Kocisko, D. A., Lansbury, P. T., and Caughey, B. (1996) Partial unfolding and refolding of scrapie-associated prion protein: Evidence for a critical 16-kDa C-terminal domain. *Biochemistry 35*, 13434–13442.